A&A 420, 929–936 (2004)
DOI: 10.1051/0004-6361:20034077

Astronomy & Astrophysics

EVN observations of H_2O masers towards the high-mass young stellar object in AFGL 5142

C. Goddi[1,2], L. Moscadelli[1], W. Alef[3], and J. Brand[4]

[1] INAF, Osservatorio Astronomico di Cagliari, Loc. Poggio dei Pini, Str. 54, 09012 Capoterra (CA), Italy
[2] Dipartimento di Fisica, Università degli Studi di Cagliari, S.P. Monserrato-Sestu Km 0.7, 09042 Cagliari, Italy
[3] Max-Planck-Institut für Radioastronomie, Auf dem Hügel 69, 53121 Bonn, Germany
[4] Istituto di Radioastronomia CNR, via Gobetti 101, 40129 Bologna, Italy

Received 15 July 2003 / Accepted 3 March 2004

Abstract. We have conducted multi-epoch EVN observations of the 22.2 GHz water masers towards the high-mass young stellar object in AFGL 5142. With four observing epochs, spanning a time of ∼1 year, 12 distinct maser features have been detected, 7 of which were detected in more than one epoch. The positions and velocities of the VLBI features agree well with those of the emission centers previously identified by means of VLA observations. For a few features, persistent over three or four epochs, accurate values of the proper motions are derived. The observed proper motions have an amplitude of 15–20 km s^{-1}, significantly larger than the range of variation of the line-of-sight velocities (±4 km s^{-1} around the systemic velocity). On the basis of their spatial distribution, the observed maser features can be divided into two groups. A model fit to the positions and velocities of the maser features of Group I, detected in the same region (within ∼500 mas) where the massive YSO should be located, demonstrates that these might arise on the surface of a nearly edge-on Keplerian disk, rotating around a massive young stellar object. The maser features of Group II, found at large distances from the YSO (≥1″), have positions and line-of-sight velocities in agreement with the blue-shifted lobe of a large-scale molecular outflow (traced by the HCO^+ and SiO emission), and might result from the interaction between the gas flowing away from the young stellar object and the ambient gas of the progenitor molecular core.

Key words. masers – stars: formation – ISM: individual objects: AFGL 5142 – ISM: kinematics and dynamics – radio lines: ISM

1. Introduction

The star formation process is better understood for low-mass stars (∼1 $M_\odot$) than for high-mass stars (≥10 $M_\odot$). The massive stars are less numerous, on average more distant from the Sun, and enter the ZAMS phase still enshrouded in their progenitor dust and gas envelope, making optical and near-infrared observations impracticable. This explains why, to date, only a handful of high-mass protostellar candidates have been identified (Cesaroni et al. 1997; Shepherd et al. 1998; Hunter et al. 1998; Molinari et al. 1998; Fontani et al. 2004). To study the formation process of massive stars, high resolution observations at radio, millimetre and far-infrared wavelenghts are needed. The highest resolutions (≤1 mas) are obtainable through the Very Long Baseline Interferometry (VLBI) technique at radio wavelenghts, which can be used to observe the maser transitions of several molecular species, such as OH, H_2O, CH_3OH, observed in the proximity of the high-mass proto-star. Multi-epoch VLBI observations can provide accurate (relative) positions, line-of-sight and transversal velocities of the maser spots (the individual, mas-scale compact, centers of emission), so that the 3-dimensional velocity distribution of the gas traced by the maser transition can be derived. Moreover, the VLBI measurements of the emission properties of the single maser spots can be usefully compared with the maser excitation models to constrain the relevant physical and geometrical parameters.

The first multi-epoch VLBI experiments were performed about 20 years ago towards a few of the strongest 22.2 GHz H_2O interstellar masers in the Galaxy, i.e. Orion-KL (Genzel et al. 1981a), W51 (Genzel et al. 1981b), Sagittarius B2 (Reid et al. 1988), W49 (Gwinn et al. 1992), and allowed both the determination of the characteristic pattern of the kinematics of these regions and, by comparing the line-of-sight velocities with the proper motions of the spots, the derivation of accurate source distances. Since then, VLBI observations of 22.2 GHz water masers have been mostly focused on those sources which, selected on the basis of interferometrical observations of (thermal) molecular tracers, are considered to be among the best high-mass protostellar candidates. The Very Long Baseline Array (VLBA) observations carried out by Moscadelli et al. (2000) towards the water masers in IRAS 20126+4104, one of the best studied examples of a

Send offprint requests to: C. Goddi,
e-mail: cgoddi@ca.astro.it

high-mass Young Stellar Object (YSO) associated with a Keplerian disk and a jet/outflow system (Cesaroni et al. 1997), suggest that the H_2O masers could arise on a bipolar conical surface, excited by the interaction of an ionized jet with the surrounding molecular gas. VLBA observations of the 22.2 GHz masers performed towards intermediate-mass (NGC 2071, Seth et al. 2002) and high-mass (IC 1396N, Slysh et al. 1999; W3 IRS 5, Imai et al. 2000) YSOs indicate that this maser emission can originate both in the protostellar disks and at the base of the molecular outflows.

This paper presents multi-epoch VLBI observations of the 22.2 GHz H_2O masers towards the high-mass star forming region AFGL 5142 (IRAS 05274+3345). At a distance of 1.8 kpc (Snell et al. 1988), its far-infrared luminosity is estimated to be 3.8×10^3 $L_\odot$ (Carpenter et al. 2002). Using the Very Large Array (VLA) at 8.4 GHz Tofani et al. (1995) have revealed a faint (1 mJy), almost unresolved, continuum source (best interpreted as free-free emission from an ionized wind), which subsequently has been found to be coincident in position with the center of a CO bipolar outflow and with the origin of a jet observed in the H_2 near-infrared emission (Hunter et al. 1995). Owens Valley Radio Observatory (OVRO) data by Hunter et al. (1999) show: 1) a well-collimated SiO-jet and an HCO^+-outflow, both aligned with the axis of the CO-outflow, and emanating from the 8.4 GHz continuum source; 2) a compact 88 GHz continuum source coincident in position (within the observational errors) with the 8.4 GHz continuum. The radio flux and the bolometric luminosity (estimated using the IRAS fluxes) can be explained if the exciting source is a massive object, with spectral type B2 or earlier. The VLA NH_3-observations performed by Zhang et al. (2002) show a $1''$ diameter (1800 AU) compact structure, whose morphology and kinematics are compatible with a rotating disk surrounding a high-mass young star.

The 22.2 GHz water masers in AFGL 5142 have been observed with the VLA at three epochs (1991, Torrelles et al. 1992; 1992, Hunter et al. 1995; 1998, Hunter et al. 1999), and found to be distributed within a few arcseconds from the 8.4 GHz continuum source. However, the VLA angular resolution ($\sim 0''.1$) is inadequate to determine the detailed spatial distribution of the maser spots, to measure their proper motions and to investigate the kinematics traced by the H_2O masers in this source. At the distance of AFGL 5142, the linear resolution attainable using the VLBI technique at 22.2 GHz is $\sim$2 AU, sufficient in principle to resolve and determine the velocity profile of a protostellar disk (of size of hundreds of AU) and/or to study the mechanism of collimation and acceleration of a jet.

Section 2 of this paper describes our multi-epoch VLBI observations and gives technical details of the data analysis, while Sect. 3 presents the observational results. Section 4 describes plausible kinematical models for interpreting the measured positions and velocities of the maser features. The conclusions are drawn in Sect. 5.

2. Observations and data reduction

AFGL 5142 was observed in the $6_{16}-5_{23}$ H_2O maser line (rest frequency 22 235.080 MHz) using the European VLBI Network (EVN) at four epochs (October 1996, and June, September, November 1997), each epoch consisting of 13 scans (of 6.5 min) distributed over an hour angle of 11 h. The antennae involved in the observations were Medicina, Cambridge, Onsala, Effelsberg, Metsahovi, Noto, Jodrell and Shanghai[1], with a subset of 5–7 of these (including always Effelsberg) observing at each epoch. Before and after each scan of AFGL 5142, several continuum sources were observed for calibration purposes (0528+134, 0642+449, 1803+784, 2251+158, 3C 454.3, OJ287). Both circular polarizations were recorded with a 1 MHz bandwidth centered on the LSR velocity of –4.8 km s^{-1}. The data were processed with the MKIII correlator at the Max-Planck-Institut für Radioastronomie (Bonn, Germany), obtaining 112 spectral channels with a separation of 0.12 km s^{-1}.

Data reduction was performed using the NRAO AIPS package, following the standard procedure for VLBI line data. Total power spectra of continuum calibrators were used to derive the bandpass response of each antenna. The amplitude calibration was performed using the information on the system temperature and the gain curve of each antenna. We did not use the "template spectrum" method (which consists of comparing total power spectra of different scans) owing to insufficient signal-to-noise ratio (SNR) of the total power spectra of the maser source.

For each observing epoch, a single scan of a strong calibrator was used to derive the instrumental (time-independent) single-band delay and the phase offset between the two polarizations. After removing the instrumental errors, all calibrator scans were fringe-fitted to determine the residual (time-dependent) delay and the fringe rate. The corrections derived from calibrators were applied to the strong maser feature used as a phase reference.

In the data analysis of each observing epoch we used as phase-reference the same maser feature at $V_{\rm LSR} = -4.8$ km s^{-1}, which exhibits a simple spatial structure consisting of a single, almost unresolved spot. The visibilities of the phase-reference channel were fringe-fitted to find the residual fringe rate produced both by differences in atmospheric fluctuations between the calibrators and the source, and by errors in the model used at the correlator. After correcting for the residual fringe rate, the visibilities of the reference channel were self-calibrated to remove any possible effects of spatial structure. Finally, the corrections derived from the reference channel were applied to data of all spectral channels.

Before producing synthesis aperture maps, we searched for maser emission in a wide field ($12'' \times 12''$) centered on the reference feature using the fringe-rate mapping method (Walker 1981). The detected emission centers, all within a few arcseconds from the phase center, were conveniently mapped by producing (naturally weighted) maps extended over a sky area of ($\Delta\alpha \cos\delta \times \Delta\delta$) $4'' \times 4''$ and covering the velocity range from -10.5 to 0.7 km s^{-1}. The CLEAN beam was an elliptical Gaussian with a typical *FWHM* size of 2.1×1.1 mas. In each observing epoch, the rms noise level

[1] The baselines to Shanghai have been almost completely flagged during the process of self-calibration.

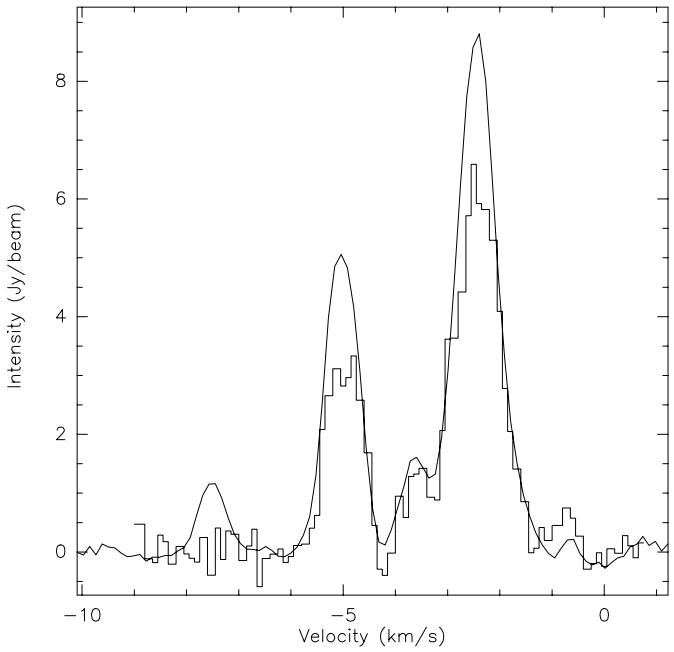

Fig. 1. The Effelsberg total-power spectrum observed in Oct. 1996 (connected plot) is compared with the integrated flux densities (histogram plot) of the VLBI channel maps. The velocity resolution of both spectra is equal to the channel width of 0.12 km s^{-1}.

on the channel maps, σ, is close to the theoretical thermal value, 0.03 Jy beam^{-1}, for channels where no signal is detected, and increases to 0.3 Jy beam^{-1} for channels with the strongest components.

Each channel map was searched for emission above a conservative detection threshold (in the range 5–10 σ), and the detected maser spots were fitted with two-dimensional elliptical Gaussians, determining position, flux density, and *FWHM* size of the emission. Hereafter, we use the term of "feature" to indicate a collection of spectrally and spatially contiguous maser spots. A maser feature is considered real if it is detected in at least three contiguous channels, with a position shift of the intensity peak from channel to channel smaller than the *FWHM* size. Figure 1 compares the Effelsberg total-power spectrum observed in Oct. 1996 with the integrated flux densities of the VLBI channel maps for the same epoch. One notes that, except for the velocity range from −7 to −8 km s^{-1}, the difference between the total-power flux and the flux recovered in the imaged VLBI field of view is within the amplitude calibration errors (±50%).

The relative positional uncertainty of the single maser spot is estimated using the expression

$$\Delta\theta = \frac{\sigma}{2I}\, FWHM, \qquad (1)$$

where *FWHM* is the un-deconvolved spot size, I is the peak intensity and σ is the no-signal rms of the map (Reid et al. 1988). For most of the spots the positional uncertainty is of the order of ∼50−100 μas.

3. Observational results

Counting all four epochs, 26 H_2O maser features were detected. Several of these show a good agreement in relative positions (within few mas) and line of sight velocities (within 1 km s^{-1}) for two or more epochs, and therefore we assume that in these cases we identified features which persist over time. A final set of 12 distinct features, 7 out of these observed for more than one epoch, has been identified.

Table 1 gives the parameters of the features, determined by fitting an elliptical Gaussian to the intensity distribution of the maser spots contributing to the features' emission at different velocity channels. Column 1 gives the feature label number. Columns 2 and 3 report respectively the line-of-sight velocity, $V_{\rm LSR}$, and the integrated flux density, $F_{\rm int}$, of the highest-intensity channel, both averaged over the observational epochs for the time-persistent features. For each feature, Cols. 4 and 5 report the positional offset (of the first epoch of detection) calculated with respect to the feature with label number "10", present at all four epochs. The positional offsets of a given feature are estimated from the (error-weighted) mean positions of the contributing maser spots. The bracketed numbers are the relative positional uncertainties, evaluated by taking the weighted standard deviation of the spot positions. With the 1−2 mas angular resolution of the EVN at 22 GHz, the emission of most of the spots is found to be spatially unresolved. Using a distance value of 1.8 kpc for AFGL 5142, an upper limit to the spot size of ∼2 AU is derived.

The proper motions have been calculated performing a (error-weighted) linear least-squares fit of the positional offsets with time. Figure 2 shows the time variation of the right ascension and declination offsets (relative to the feature "10") for the persistent features. Among the features observed at three or more epochs, the proper motions are derived only for those moving in a straight line at constant velocity (identified with the label numbers "2", "6" and "12"). Tentative values of the proper motions are calculated also for the two features (with label number "1" and "11") observed at only two epochs. Columns 6–8 of Table 1 report respectively the projected components along the RA and Dec axis, and the absolute value of the derived proper motions. The numbers in italics refer to features observed at only two epochs. The bracketed numbers are the formal errors of the linear least-squares fit.

Figure 3 compares our VLBI results with previous interferometric observations. Top panels show the high-velocity molecular outflows seen in HCO^+ ($1 \rightarrow 0$) and SiO ($v = 0$, $2 \rightarrow 1$) with OVRO (Hunter et al. 1999). The area comprising almost the totality of the 22.2 GHz water maser emission detected by our VLBI observations, is indicated by a small filled rectangle at the center of the field of view. This area is expanded in the lower panel of Fig. 3, which shows the spatial distribution of the VLBI maser features superimposed on top of the distribution of the VLA emission centers found by Hunter et al. (1995, 1999) at two different epochs. The measured proper motions are indicated by the arrows.

The absolute position of the VLBI map has been determined by aligning the VLBI and VLA maser emission centers. The VLBI map has been shifted on top of the VLA map to find

Table 1. Maser feature parameters.

	Feature	$V_{\rm LSR}$ (km s^{-1})	$F_{\rm int}$ (Jy)	$\Delta\alpha$ (mas)	$\Delta\delta$ (mas)	V_x (km s^{-1})	V_y (km s^{-1})	$V_{\rm mod}$ (km s^{-1})
	1	–7.2	16.9	189.7 (0.3)	1020.7 (0.2)	*23.7 (12.6)* †	*–33.8 (8.2)*	*41.2 (9.9)*
	2	–4.8	5.9	157.7 (0.2)	1010.43 (0.03)	4.2 (1.8)	–15.2 (0.4)	15.8 (0.6)
	3	–4.8	0.5	157.3 (0.2)	1012.1 (0.2)			
Group I	4	–3.6	0.8	159.0 (0.2)	1017.26 (0.03)			
	5	–2.0	4.1	–32.5 (0.2)	1290.15 (0.09)			
	6	–1.2	1.0	174.3 (0.3)	1007.5 (0.2)	4.4 (2.7)	–19.1 (1.3)	19.6 (1.4)
	7	–0.6	0.3	28.7 (0.2)	1251.03 (0.07)			
	8	0.7	0.3	55.5 (0.2)	1245.85 (0.08)			
	9	–5.4	0.3	–50.3 (0.3)	–18.99 (0.02)			
Group II	10	–5.2	4.8	0.00	0.00	0.00	0.00	0.00
	11	–3.9	3.0	–655.2 (0.3)	–566.7 (0.1)	*–25.3 (15.0)*	*–9.8 (4.8)*	*27.1 (14.1)*
	12	–3.7	1.2	–179.3 (0.2)	–75.6 (0.1)	–1.0 (1.9)	0.6 (1.3)	1.2 (1.8)

† The italics indicate tentative values of proper motion components for features observed at only two epochs.

a shift that minimizes the root mean square difference between the positions of the VLBI and VLA spots. We find that each of the detected VLBI features has a good positional (within the VLA beam of ∼100 mas) and line-of-sight velocity correspondence with one of the observed VLA spots. Conversely, we have detected VLBI features corresponding to each VLA emission center with peak flux density ≥0.4 Jy. The good overlap found between the VLBI and the VLA emission makes us confident that the absolute position derived for the VLBI map is accurate within the VLA positional uncertainty.

On the basis of their spatial distribution, the VLBI maser features can be divided into two groups. Group I, comprising the first eight features, is found in the northeast corner of the area plotted in the lower panel of Fig. 3, in the same region (within ∼500 mas) where the 8.4 GHz and 88 GHz continuum emissions are detected. Group II includes the last four maser features more detached (≥1″) from the continuum emissions, extending towards the south and the southwest corner of the plotted area.

Figure 3 and Table 1 of Hunter et al. (1999) show that at epoch 1998 two VLA emission centers (their components "6" and "7") are detected at positions separated about 3–4″ from the 8.4 GHz continuum peak. We produced VLBI maps also at these two locations, toward both directions detecting a single, weak (≤Jy beam^{-1}) spot in the last two epochs (September and November 97). No features persisted over time and, consequently, no proper motions are measured. The components "6" and "7" were among the strongest ones in the epoch 1998 VLA observations of Hunter et al. (1999) but were not detected in the two prior VLA epochs (1991, Torrelles et al. 1992; 1992, Hunter et al. 1995). Our VLBI observations, extending over the years 1996 and 1997, fall in between the 1992 (Hunter et al. 1995) and 1998 (Hunter et al. 1999) VLA runs, and record the first appearance of water maser emission in these two regions. Being detached from the 8.4 GHz and 88 GHz sources, the maser emission in these two locations very likely traces a site of star formation other than the one responsible for the line and continuum emission shown in Fig. 3. A single maser spot does not allow us to derive information on the gas kinematics and we will not consider these two regions further in the following discussion.

4. Discussion

Figure 3 shows that the spatial distribution of all the VLBI and VLA maser features is extended along a north−south direction. The outflow detected in the CO, HCO^+ and SiO emission has a similar orientation (Hunter et al. 1995, 1999). In addition, although the line-of-sight velocities of the VLBI maser features do not vary smoothly, the mean velocity of the Group I cluster (toward the north) is more positive (redshifted) than that of the Group II (toward the south). Over an area of sky slightly larger than that plotted in Fig. 3, a similar variation of the line-of-sight velocities (more redshifted (blueshifted) toward the North (South)) is also noteable in the VLA 22 GHz observations of Hunter et al. (1999; their Table 1), where the most northward VLA maser components (labeled "9"–"11" in Hunter et al. 1999) occur at velocities (≥−1 km s^{-1}) higher than the most southwarth components (labeled "2" and "8" in Hunter et al. 1999) (≤−3 km s^{-1}). The observed variation of water maser velocity is qualitatively in agreement with the velocity distribution seen at a much larger angular scale in the HCO^+ and SiO maps (Fig. 3). A simple interpretation might be that all the detected (VLA and VLBI) maser features are tracing the flow motion in the innermost portion of the molecular outflow. To make the discussion more quantitative, considering that the line-of-sight velocity dispersion of the large-scale (diameter ∼50″) molecular outflow is ∼100 km s^{-1}, and

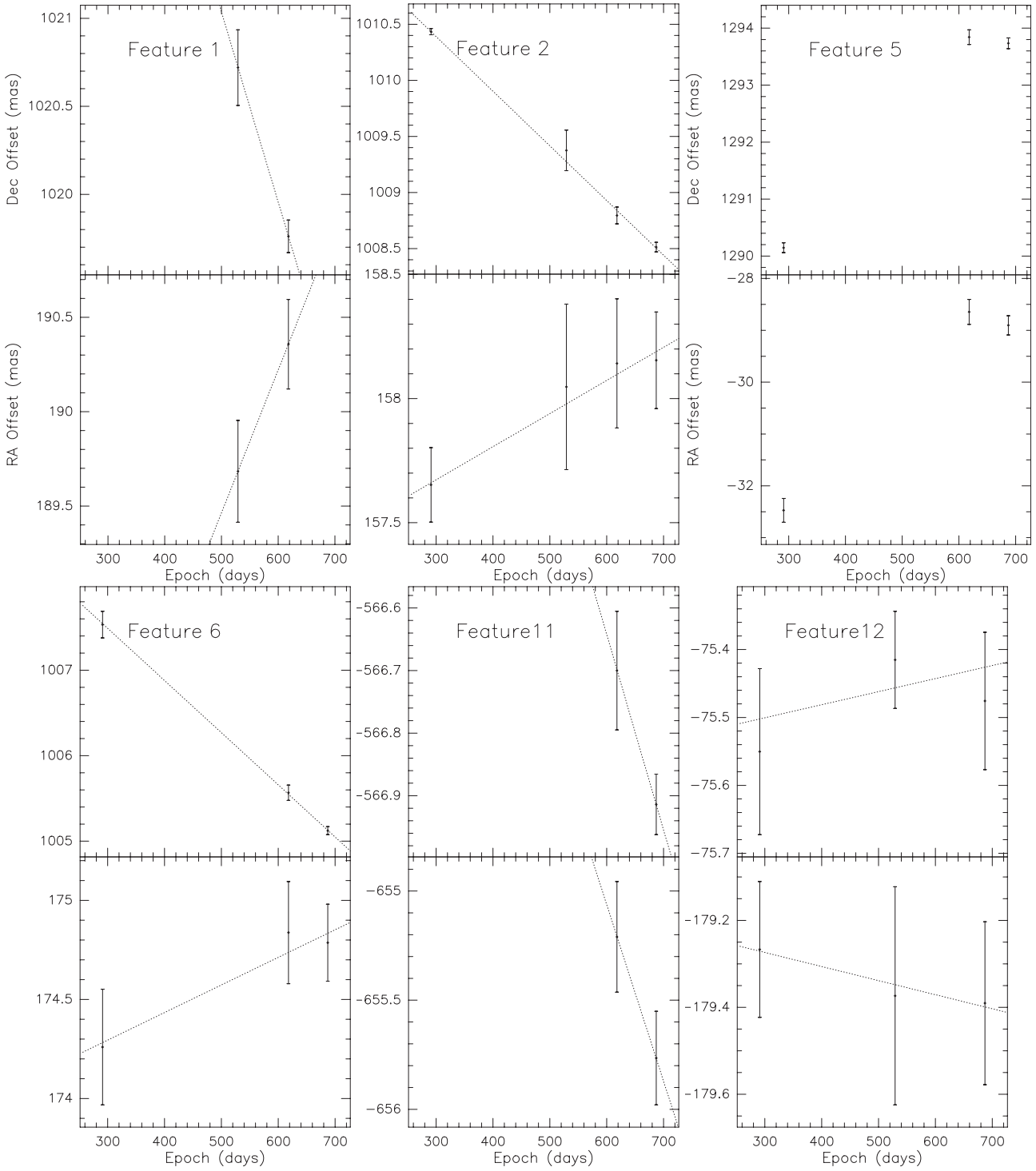

Fig. 2. Measured relative proper motions of H_2O maser features in AFGL 5142. For each of the time persistent features, the top and the bottom panels report the time variation of respectively the declination and the right ascension offsets (relative to the feature "10"). In each panel, the dotted line shows the proper motion calculated by the (error-weighted) linear least-squares fit of the positional offsets with time. Among the features observed at three or more epochs, the proper motions are derived only for those moving in a straight line at constant velocity (within the positional errors). Adopting such a criterion, no proper motion is derived for feature "5". Tentative values of the proper motions are calculated also for the two features (label number "1" and "11") observed at only two epochs.

assuming a Hubble flow (velocity increasing linearly along the outflow axis), one would derive a rate of line-of-sight velocity dispersion caused by the outflow of ~2 km s^{-1} arcsec^{-1}. If that might explain the velocity dispersion of the Group II features (1.7 km s^{-1} over a distance of 1″; see Table 1), the Group I features show a much higher velocity dispersion (8 km s^{-1}) across a smaller distance (0.″35).

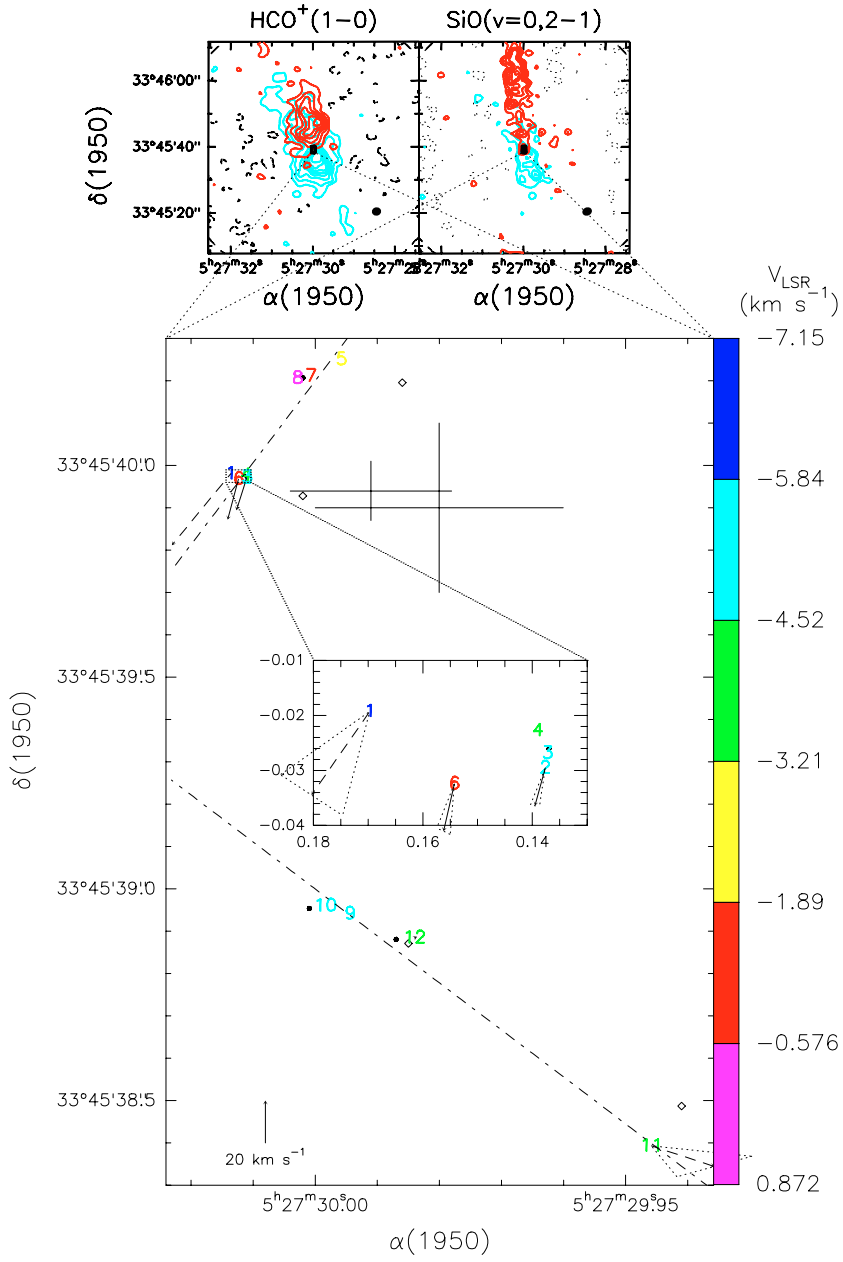

Fig. 3. The upper panels show the contour maps of the high-velocity molecular line emission of HCO^+ ($1 \rightarrow 0$) (*left*) and SiO ($v = 0, 2 \rightarrow 1$) (*right*), observed with OVRO in 1998 by Hunter et al. (1999; their Fig. 10). The area at the center of the OVRO field of view, where most of the 22.2 GHz water emission detected by our VLBI observations is concentrated, is expanded in the lower panel. This shows the spatial distribution of the VLBI features superimposed on top of the distribution of the VLA emission centers found by Hunter et al. (1995, 1999) at the two different epochs (1992, open diamonds; 1998, filled dots). Each VLBI feature is identified with the label number given in Col. 1 of Table 1. Different colours are used to distinguish the line of sight velocities of the features, according to the colour-velocity conversion code shown on the right-hand side of the panel. The arrows indicate the measured proper motions, with dashed lines used in case of more uncertain values. The dotted triangles drawn around the proper motion vectors represent the amplitude and orientation uncertainty. The region in the northeast corner enclosed by the dotted lines is shown in greater detail in the box at the center of the lower panel, whose coordinates are arcsec offsets relative to the position: RA = $05^h27^m30^s$; Dec = $+33°45'40''$. For the feature labeled "12", with a small measured value of the proper motion, cannot be assigned a definitive direction of motion. The amplitude scale for the proper motions is given at the bottom left corner of the panel. The small and the big crosses give respectively the position uncertainties of the VLA 8.4 GHz and the OVRO 88 GHz continuum emission peaks (Hunter et al. 1999). For each of the two Groups of EVN maser features, the black dot-dashed line indicates the axis whose average distance from the feature positions is minimum.

The maser features of Group I have a sky-projected distance $\leq$500−1000 AU from the 8.4 GHz and 88 GHz continuum sources, and should emerge near to the expected location of the massive YSO. At such a close distance to the YSO, it might be possible that the flow motion has not yet reached a stable configuration and turbulence might play a role in increasing

the velocity dispersion of the gas. Alternatively, the maser features of Group I might move under the influence of the gravitational field of the massive YSO. Within a region of radius of ∼1000 AU around the forming high-mass star, the current theory of star formation predicts that an accretion disk should be found. Looking at Fig. 3, one notes that the maser features of Group I have an elongated spatial distribution (the dot-dashed line indicates the elongation axis) and that the measured proper motions have an orientation close to that of the elongation axis. This geometrical condition is what one would in principle expect if these maser features traced a rotating disk seen edge-on. However, one should note that the derived proper motions are relative to the feature "10" (not belonging to the Group I maser cluster), and, in order to obtain the absolute transversal velocities of the gas, one has to correct for the (unkwown) absolute motion of this feature.

Even if only a small number of maser features is detected toward the Group I cluster, our accurate knowledge of their positions and line-of-sight velocities offers the chance to fit their motion using a 3-D Keplerian disk model. The model's free parameters are: the sky-projected coordinates of the YSO (at the disk center); the position angle and the inclination angle with the line-of-sight of the disk axis; the YSO mass. For a given set of input parameters, one can compute the position and the velocity vector of each feature and compare the model velocities with the observed velocities. The best fit to the data was obtained minimizing the χ^2 given by the squared sum of the error-weighted differences of the model and observed line-of-sight velocities. Incidentally we note that the same fit solution is found when the χ^2 is calculated including also the two measured proper motions (for the features labelled "2" and "6" in Table 1).

Looking for the disk axis orientation over the full 4π solid angle, the best fit solution is found with the disk seen almost edge-on (inclined 12° from the line-of-sight) and oriented on the sky parallel to the elongation axis of the Group I features (at PA = 153°). The fitted value of the YSO mass, $M_{\rm YSO} = 38\ M_\odot \pm 20\ M_\odot$, although determined with high uncertainty, strongly indicates that the central object is a massive YSO ($M > 10\ M_\odot$). This result is in agreement with that of previous observations (Hunter et al. 1995, 1999), indicating an exciting object of spectral type B2 or earlier, for which the theoretically expected value of the mass is $\geq$10 $M_\odot$ (Vacca et al. 1996; Palla & Zinnecker 2002). Adopting a distance of 1.8 kpc to AFGL 5142, the range of disk radii traced in our model by the maser emission extends from ∼30 AU to ∼800 AU, which is consistent with the size of several hundreds of AU expected for an accreting disk around a massive YSO. From the barely resolved 88 GHz emission, interpreted in terms of optically thin thermal emission from a dusty core, Hunter et al. (1999) derive a core size of ∼5000 AU and a core mass of ∼145 $M_\odot$. These values are compatible with the results of our model, which tells us that within a radius of ∼1000 AU the mass in Keplerian motion is $\lesssim$60 $M_\odot$.

Recently Zhang et al. (2002) have observed the high-mass star-forming region AFGL 5142 in several NH_3 inversion transitions using the VLA array. In correspondence to the 88 GHz source of Hunter et al. (1999), they find a compact (1″ in diameter), hot (70 K), NH_3 structure, with a broad line emission, interpreted as an unresolved rotating disk. Looking at Fig. 2 of Zhang et al. (2002), one sees that the velocity range (from −8 km s^{-1} to 2 km s^{-1}) over which the NH_3 "disk" emission is detected matches well with the velocity range of the Group I maser emission. The value of the "disk" mass estimated from the NH_3 measurements of Zhang et al. (2002) is 4 $M_\odot$, assuming an NH_3 abundance (relative to H_2) of 10^{-6}. This value of the "disk" mass, being much lower than the fitted YSO mass (38 $M_\odot$), is compatible with the Keplerian disk model proposed to explain the kinematics of the 22 GHz maser features that we observed.

Owing to their large distance (2000–3000 AU) from the YSO believed to be responsible for the continuum emissions and the acceleration of the large scale molecular ouflow, the Group II of maser features also might be associated with a distinct (as yet undetected) YSO. However, the fact that the positions and the radial velocities of these features are in agreement with the blue-shifted lobe of the molecular outflow makes us favour the intepretation that their emission is excited by the interaction of the gas outflowing from the YSO with the ambient gas of the progenitor molecular core. Looking at Fig. 3 one notes that the spatial distribution of the maser features of Group II is elongated (the dot-dashed line indicates the elongation axis) along a direction (at PA = 44°) that differs from that of the large scale HCO^+ and SiO outflows, oriented approximately north-south. Towards the infrared sources IRS1 and IRS3 in the NGC 2071 star-forming region, Seth et al. (2002) note similar differences of orientation between the outflow structures on large (>1000 AU) and small (10−100 AU) scales. This effect might be explained by either the density gradients in the ambient medium, causing large-angle bends of the protostellar jets, or multiple, small scale outflows, whose merging creates the large scale flow.

5. Conclusions

Using the EVN we have observed the 22.2 GHz H_2O masers towards the massive star forming region AFGL 5142 for four epochs (from October 1996 to November 1997). Previous high-angular resolution observations of several thermal tracers in the cm and mm-wavelength band indicate that the exciting source of the water maser emission is a high-mass YSO, of spectral type B2 or earlier.

We identified a final set of 12 distinct water maser features, 7 out of these detected in more than one epoch. For a few features, persistent over three or four epochs, accurate values of the proper motions are derived. The observed proper motions have amplitudes of 15−20 km s^{-1}, significantly larger than the range of variation of the line-of-sight velocities (±4 km s^{-1} around the systemic velocity). The positions and the velocities of the VLBI features agree well with those of the emission centers previously identified by means of VLA observations.

On the basis of their spatial distribution, we have divided the maser features into two groups. Group I, comprising eight VLBI features, is found in the same region (within ∼500 mas) where the massive YSO, believed to be the exciting source of two compact continuum sources (at 8.4 GHz and 88 GHz),

should be located. A model fit to the positions and velocities of these features indicates that they might arise on the surface of a Keplerian disk seen nearly edge-on. The fitted value of the YSO mass, $M_{\rm YSO} = 38\ M_{\odot} \pm 20\ M_{\odot}$, although determined with high uncertainty, is in agreement with the results of previous observations. Maser features of Group II, found at larger distances ($\geq 1''$) southward from the YSO, have positions and line-of-sight velocities in agreement with the blue-shifted lobe of a large-scale molecular outflow (detected in the HCO^+ and SiO emission), and might be excited by the interaction of the gas outflowing from the YSO with the ambient gas of the progenitor molecular core.

This work demonstrates that multi-epoch EVN observations are able to measure the proper motions of the strongest and longer-living 22.2 GHz maser features. Our EVN observations towards the source AFGL 5142 suffered two major drawbacks: 1) the time separation between consecutive epochs ($\geq$3 months) is too long compared to the average life time of the maser features; 2) modest sensitivity (with an average detection threshold of $\sim$0.35 Jy beam^{-1}), owing to the fact that only 5−7 antennae (out of the 11 available to observe at 22.2 GHz) took part in each run. Next we plan to use the VLBA to better constrain the kinematical scenario suggested by the EVN observations, using a shorter time separation ($\sim$1 month) between two consecutive epochs and higher sensitivity.

Acknowledgements. The European VLBI Network is a joint facility of European, Chinese, South African and other radio astronomy institutes funded by their national research councils. We are very gratful to L. Testi for providing the plots of the molecular outflows.

References

Carpenter, J. M., Snell, R. L., & Schloerb, F. P. 2002, ApJ, 362, 147
Cesaroni, R., Felli, M., Testi, L., Walsmley, C., & Olmi, L. 1997, A&A, 325, 725
Fontani, F., Cesaroni, R., Testi, L., et al. 2004, A&A, 414, 299
Genzel, R., Reid, M. J., Moran, J. M., & Downes, D. 1981a, ApJ, 244, 884
Genzel, R., Downes, D., Schneps, M. H., et al. 1981b, ApJ, 247, 1039
Gwinn, C. R., Moran, J. M., & Reid, M. J. 1992, ApJ, 393, 149
Hunter, T., Neugebauer, G., Benford, D., et al. 1998, ApJ, 493, L97
Hunter, T., Testi, L., Taylor, G., et al. 1995, A&A, 302, 249
Hunter, T., Testi, L., Zhang, Q., & Sridharan, T. 1999, AJ, 118, 477
Imai, H., Kameya, O., Sasao, T., et al. 2000, ApJ, 538, 751
Molinari, S., Testi, L., Brand, J., Cesaroni, R., & Palla, F. 1998, ApJ, 505, L39
Moscadelli, L., Cesaroni, R., & Rioja, M. J. 2000, A&A, 360, 663
Palla, F., & Zinnecker, H. 2002, Physics of Star Formation in Galaxies, Saas-Fee Advanced Course 29, Les Diablerets, Switzerland, 22 to 29 March 1999, ed. A. Maeder, & G. Meynet (Berlin: Springer Verlag), 102
Reid, M. J., Schneps, M. H., Moran, J. M., et al. 1988, ApJ, 330, 809
Seth, A., Greenhill, L. J., & Holder, B. P. 2002, ApJ, 581, 325
Shepherd, D., Watson, A., Sargent, A., & Churchwell, E. 1998, ApJ, 507, 861
Slysh, V. I., Val'tts, I. E., Migenes, V., et al. 1999, ApJ, 526, 236
Snell, R. L., Huang, Y.-L., Dickman, R. L., & Claussen, M. J. 1988, ApJ, 325, 853
Tofani, G., Felli, M., Taylor, G., & Hunter, T. 1995, A&AS, 112, 299
Torrelles, J. M., Gomez, J. F., Anglada, G., et al. 1992, ApJ, 392, 616
Vacca, W. D., Garmany, C. D., & Shull, J. M. 1996, ApJ, 460, 914
Walker, R. 1981, AJ, 86, 1323
Zhang, Q., Hunter, T., Sridharan, T., & Ho, P. 2002, ApJ, 566, 982